Nitazoxanide and JIB-04 have broad-spectrum antiviral activity and inhibit SARS-CoV-2 replication in cell culture and coronavirus pathogenesis in a pig model

Juhee Son[1,2,*], Shimeng Huang[3,*], Qiru Zeng[1,*], Traci L. Bricker[4], James Brett Case[4], Jinzhu Zhou[3], Ruochen Zang[1,5], Zhuoming Liu[1], Xinjian Chang[3], Houda H. Harastani[4], Lu Chen[6], Maria Florencia Gomez Castro[1], Yongxiang Zhao[3], Hinissan P. Kohio[1], Gaopeng Hou[1], Baochao Fan[3], Beibei Niu[3], Rongli Guo[3], Paul W. Rothlauf[1,7], Adam L. Bailey[8], Xin Wang[5], Pei-Yong Shi[9], Sean P.J. Whelan[1], Michael S. Diamond[1,4,8], Adrianus C.M. Boon[1,4,8], Bin Li[3,#], Siyuan Ding[1,#]

[1]Department of Molecular Microbiology, Washington University School of Medicine, St. Louis, MO, USA. [2]Program in Molecular Cell Biology, Washington University School of Medicine, St. Louis, MO, USA. [3]Institute of Veterinary Medicine, Jiangsu Academy of Agricultural Sciences, Nanjing, China. [4]Department of Medicine, Division of Infectious Diseases, Washington University School of Medicine, St. Louis, MO, USA. [5]Key Laboratory of Marine Drugs, Ministry of Education, Ocean University of China, Qingdao, China. [6]National Center for Advancing Translational Sciences, National Institutes of Health, Rockville, MD, USA. [7]Program in Virology, Harvard Medical School, Boston, MA, USA. [8]Department of Pathology and Immunology, Washington University School of Medicine, St. Louis, MO, USA. [9]Department of Biochemistry and Molecular Biology, University of Texas Medical Branch, Galveston TX, USA.

* These authors contributed equally: Juhee Son, Shimeng Huang, Qiru Zeng

24 # Corresponding authors: Bin Li, libinana@126.com, Siyuan Ding, siyuan.ding@wustl.edu

25

26 **Abstract**

27

28 Pathogenic coronaviruses represent a major threat to global public health. Here, using a
29 recombinant reporter virus-based compound screening approach, we identified several
30 small-molecule inhibitors that potently block the replication of the newly emerged severe
31 acute respiratory syndrome virus 2 (SARS-CoV-2). Two compounds, nitazoxanide and
32 JIB-04 inhibited SARS-CoV-2 replication in Vero E6 cells with an EC_{50} of 4.90 μM and
33 0.69 μM, respectively, with specificity indices of greater than 150. Both inhibitors had *in*
34 *vitro* antiviral activity in multiple cell types against some DNA and RNA viruses, including
35 porcine transmissible gastroenteritis virus. In an *in vivo* porcine model of coronavirus
36 infection, administration of JIB-04 reduced virus infection and associated tissue pathology,
37 which resulted in improved body weight gain and survival. These results highlight the
38 potential utility of nitazoxanide and JIB-04 as antiviral agents against SARS-CoV-2 and
39 other viral pathogens.

40

41 **INTRODUCTION**

42

43 The coronavirus disease 2019 (COVID-19) pandemic has caused unprecedented global
44 morbidity, mortality, and socioeconomic destabilization. Thus, there is an urgent unmet
45 need to develop safe and effective countermeasures to combat the disease and provide
46 immediate treatment. Multiple efforts are underway to identify candidate drugs that inhibit

47 the replication of the novel severe acute respiratory syndrome virus 2 (SARS-CoV-2) (*1-*
48 *5*), the cause of COVID-19 (*6, 7*). So far, several small-molecule inhibitors that interfere
49 with SARS-CoV-2 cell entry have been identified, including transmembrane serine
50 protease inhibitors camostat (*8*) and nafamostat (*9*), and endosomal inhibitors including
51 chloroquine and derivatives (*9*), E-64d (*8*), apilimod (*10*), and 25-hydroxycholesterol (*11*).
52 Drug screens and structural studies also revealed compounds that target SARS-CoV-2
53 viral enzymes such as the viral RNA-dependent RNA polymerase (RdRp) (*12-14*) and the
54 main protease (M^{pro}, also known as $3CL^{pro}$) (*15-17*). Here, utilizing a fluorescent SARS-
55 CoV-2 virus and an imaging-based screen approach, we identified several known and
56 previously unknown broadly antiviral compounds that successfully inhibit SARS-CoV-2
57 replication.
58
59 **RESULTS**
60
61 To identify small molecules with anti-SARS-CoV-2 activity, we performed a screen with a
62 recombinant SARS-CoV-2 that encodes mNeonGreen as a reporter of infection (*18*) and
63 an in-house collection of ~200 compounds that comprise FDA-approved drugs, well-
64 defined broad-spectrum antivirals, and investigational new drugs. We identified
65 molecules with stronger antiviral efficacy (>44.8% inhibition) than the positive controls
66 chloroquine and remdesivir against SARS-CoV-2 replication in Vero E6 cells (**Fig. 1A** and
67 **Dataset S1**).
68

69 We selected two small molecules for detailed characterization: [2-[(5-nitro-1,3-thiazol-2-
70 yl)carbamoyl]phenyl] acetate (nitazoxanide, abbreviated as NTZ), an FDA-approved drug
71 for treatment of diarrhea caused by *Giardia lamblia* and *Cryptosporidium parvum*
72 infections (*19*), and 5-chloro-N-[(E)-[phenyl(pyridin-2-yl)methylidene]amino]pyridin-2-
73 amine (JIB-04 E-isomer), a pan-Jumonji histone demethylase inhibitor (*20*) (**Fig. S1A**).
74 NTZ was chosen based on its broad-spectrum antiviral activity against several respiratory
75 viruses (rhinovirus A, influenza A virus, human metapneumovirus and respiratory
76 syncytial virus) (https://drugvirus.info/) and safety profile in humans. NTZ is currently
77 being tested in clinical trials for COVID-19 in Mexico and Brazil (ClinicalTrials.gov
78 identifiers: NCT04341493; NCT04348409). However, no pre-clinical data is published to
79 support an *in vitro* inhibitory function. JIB-04 was picked for its stronger anti-SARS-CoV-
80 2 activity than NTZ (**Fig. S1B**). Moreover, it has not been reported as an antiviral molecule
81 before and several histone demethylases were recently uncovered in a CRISPR/Cas9
82 genetic knockout screen of SARS-CoV-2 host dependency factors (*21*).
83
84 We confirmed that pre-treatment of cells with either NTZ or JIB-04 for 1 hr inhibited the
85 replication of a clinical isolate of SARS-CoV-2 (2019-nCoV/USA-WA1/2020 strain) by
86 viral antigen staining in Vero E6 cells (**Fig. 1B**). In Vero E6 cells, NTZ and JIB-04 had
87 half-maximal effective concentration (EC_{50}) values of 4.90 μM (with 95% confidence
88 interval of 3.05-7.25 μM) and 695 nM (with 95% confidence interval of 567-822 nM),
89 respectively. Both drugs did not induce cytotoxicity at 300 μM and thus had excellent
90 selectivity indices (SI > 150). Intracellular SARS-CoV-2 RNA levels also were reduced
91 significantly by NTZ and JIB-04 but not by camostat treatment (**Fig. 1C**).

92

93 To examine whether the lead compounds target cellular pathways (e.g., entry, translation,
94 replication, or assembly) shared by different viruses, we counter-screened 15 molecules
95 with a vesicular stomatitis virus (VSV) eGFP virus (*22*) and a replication-competent
96 chimeric VSV eGFP virus that encodes SARS-CoV-2 spike (S) protein in place of the
97 native glycoprotein (*23*). Concanamycin A and MG132 preferentially (>50-fold) inhibited
98 VSV-SARS-CoV-2 than VSV, implying that at least part of the antiviral activity was
99 specific to the S protein (**Fig. 2A**). In contrast, the majority of the top hits from the drug
100 screen (thapsigargin, AG-1478, FTY720, 3-isobutyl-1-methylxanthine (IBMX), arbidol,
101 nigericin, JIB-04, and nitazoxanide) suppressed both VSV and VSV-SARS-CoV-2
102 replication in MA104 cells (**Fig. 2A**). Using flow cytometry, we observed that NTZ or JIB-
103 04 reduced the infectivity of VSV and VSV-SARS-CoV-2 at 6 hr post infection (hpi), within
104 a single replication cycle (**Fig. 2B**). Less GFP intensity was detected in infected cells (**Fig.
105 S2A**), suggesting that the inhibitors might act on a common post-entry pathway. NTZ or
106 JIB-04 reduced VSV-SARS-CoV-2 replication in a dose-dependent manner without
107 apparent cytotoxicity (**Fig. 2C** and **S2B**). The inhibitory effects were more apparent when
108 cells were infected with VSV-SARS-CoV-2 at a low multiplicity of infection (MOI) (**Fig.
109 S2C**). At 30 μM, JIB-04 treatment led to 100-fold reduction of intracellular VSV-SARS-
110 CoV-2 RNA levels, comparable to the efficacy of chloroquine (**Fig. S2D**).

111

112 Unlike NTZ, with reported broad-spectrum antiviral activity (*24-27*), JIB-04 is not known
113 to have an antiviral function. We found that besides VSV (**Fig. 2A**), JIB-04 had antiviral
114 property against both DNA and RNA viruses, including vaccinia virus and two strains of

115 rotaviruses (RVs) (**Fig. 2D**). JIB-04 also inhibited the replication of enteric viruses, i.e. a
116 strain of porcine RV and transmissible gastroenteritis virus (TGEV) (**Fig. 2E-F** and **Fig.**
117 **S2E**), a porcine CoV that infects the small intestine of pigs and causes severe diarrheal
118 disease (*28*).
119
120 Ciliated airway epithelial cells are a target for SARS-CoV-2 *in vivo* (*29*), and the human
121 lung epithelial cell line, Calu-3, has been used to evaluate SARS-CoV-2 infection as an
122 *in vitro* surrogate (*8, 30*). NTZ inhibition of VSV-SARS-CoV-2 replication, as measured by
123 viral RNA levels, was ineffective in HEK293-hACE2-TMPRSS2 and Calu-3 cells, in
124 contrast to JIB-04 (**Fig. 2G**), suggesting distinct antiviral mechanisms.
125
126 Although NTZ and JIB-04 have been previously connected to interferon (IFN) and
127 autophagy activation (*20, 31, 32*), the antiviral activity that we observed was independent
128 of these pathways. Neither treatment led to the induction of IFN and IFN-stimulated gene
129 expression or the formation of LC3-positive punctate structures (**Fig. S3A-B**). Using a
130 dose-response drug matrix, we found that JIB-04 had synergistic antiviral effects with
131 chloroquine and NTZ in MA104 cells (**Fig. 3A**). Synergism was calculated by the highest
132 single agent (HSA) synergy model using SynergyFinder 2.0 (*33*). JIB-04 at 0.1-3 μM had
133 the most synergy with either chloroquine or NTZ at 1-10 μM (**Fig. 3A**). A combinatorial
134 effect of JIB-04 and camostat also was observed in Calu-3 cells (**Fig. S3C**), further
135 highlighting a unique antiviral mode of action of JIB-04.
136

137 Time of addition experiments also supported that both NTZ and JIB-04 primarily acted at
138 a post-entry step (**Fig. 3B**). Pre-incubation of the cells with JIB-04 for 1 hr significantly
139 reduced SARS-CoV-2 S mRNA transcription post VSV-SARS-CoV-2 infection (**Fig. 3C**).
140 Consistently, the newly synthesized full-length S protein levels were strongly decreased
141 (**Fig. 3D**). We obtained similar results with SARS-CoV-2 plasmid transfection. JIB-04
142 treatment suppressed S mRNA transcription (**Fig. S3D**) and almost completely prevented
143 the production of full-length and protease-processed SARS-CoV-2 S proteins (**Fig. S3E**).
144
145 In parallel, we examined the cellular signaling pathways modulated by JIB-04. Small
146 interfering RNA (siRNA)-mediated knockdown of JIB-04 cellular targets (*i.e.*, histone
147 demethylases KDM4B, KDM4C, KDM5A, or KDM5B (*20*)) recapitulated the antiviral effect
148 of JIB-04 (**Fig. 3E** and **Fig. S3F-G**). We hypothesized that JIB-04 treatment led to H3K9
149 and H3K27 methylation and silenced expression of a subset of genes. To evaluate this
150 idea, we performed RNA-sequencing on mock and JIB-04 treated cells with or without
151 virus infection to identify the potential JIB-04 targets. Pathway analysis revealed
152 dampened metabolic signaling such as the cytochrome P450 system in JIB-04 treated
153 cells (**Fig. S3H**). Specifically, JIB-04 downregulated two cytochrome P450 enzymes,
154 *CYP1A1* and *CYP1B1*, and aryl hydrocarbon receptor repressor (*AHRR*), product of
155 which represses transactivator of CYP1A1 and CYP1B1 (*34*) (**Fig. 3F**). We validated by
156 quantitative PCR that JIB-04 treatment reduced *CYP1A1*, *CYP1B1*, and *AHRR* mRNA
157 levels by 4-6-fold (**Fig. 3G**). To explore the pharmacological utility of this finding, we tested
158 the antiviral activity of cytochrome P450 enzyme inhibitors Fluoxetine and Fluvoxamine

159 (*35*). Both compounds inhibited the replication of VSV-SARS-CoV-2 (**Fig. 3H**) and wild-
160 type SARS-CoV-2 (**Fig. 3I**).
161
162 Next, we used a neonatal pig TGEV infection model (*36*) to assess the antiviral efficacy
163 of JIB-04 against coronavirus *in vivo*. Two-day old piglets were injected via intraperitoneal
164 route with JIB-04 at 24 hr and 6 hr before oral inoculation of TGEV (**Fig. 4A**). We
165 monitored body weight on a daily basis and recorded diarrhea development and mortality
166 every 6 hr. The animals in the control group lost more weight and had more severe
167 diarrhea than those receiving JIB-04 (**Fig. S4A-B**). At 2 days post infection, 3 out of 5
168 piglets in the DMSO group succumbed to infection as compared to 1 out of 5 animals in
169 the JIB-04 group (**Fig. 4B**). Consistent with our *in vitro* results (**Fig. 2E-F**), the TGEV viral
170 loads throughout the gastrointestinal tract, measured by viral RNA and titer levels, were
171 substantially lower in the JIB-04 treated piglets (**Fig. 4C-D**). The number of viral antigen
172 positive intestinal epithelial cells also was decreased following JIB-04 treatment (**Fig.**
173 **S4C**). Independent of virus inhibition, JIB-04 enhanced the expression of tight-junction
174 genes such as claudin-1 and ZO-1 and pro-inflammatory cytokines including IFN-β and
175 TNF-α (**Fig. S4D-E**). Furthermore, we observed less severe enteropathy in the JIB-04
176 treated animals (**Fig. 4E**). Taken together, our data demonstrate *in vivo* antiviral activity
177 of JIB-04 against a major porcine CoV pathogen.
178
179 **DISCUSSION**
180

181 Using a repurposed compound screening approach, we identified drugs with reported
182 inhibitory activity against SARS-CoV-2, such as tetrandrine (*37*) and arbidol (*38*), and
183 characterized a number of previously unreported small-molecule (JIB-04, AG-1478,
184 nigericin, etc.) that reduced SARS-CoV-2 infection. Several compounds converge on the
185 endosomal pathway: brefeldin A, concanamycin A, tetrandrine, and U18666A.
186 Furthermore, FTY720 induced formation of enlarged endosome/lysosome structure,
187 similar to that triggered by apilimod treatment (*39*), highlighting an important role of
188 endosomal trafficking in SARS-CoV-2 entry and infection, at least in cell culture.
189
190 Our results highlight NTZ and JIB-04 as potential therapeutics for SARS-CoV-2 and the
191 need for further evaluation. Compared to NTZ, JIB-04 does not have reported antiviral
192 properties. Another compound in our screen, GSK-J4, also is a histone demethylase
193 inhibitor, which targets JMJD3/KDM6B. However, it did not inhibit SARS-CoV-2
194 replication. Thus, a definitive involvement of certain KDM family members in SARS-CoV-
195 2 host interactions has not been established.
196
197 Although NTZ has been used to treat protozoan infections since 1984 (*40*), the
198 mechanisms underlying its anti-microbial activities are not fully elucidated. Our *in vitro*
199 results support a post-entry inhibitory mode of action, which was previously proposed for
200 hepatitis C virus (*27*). In a non-placebo-controlled setting, NTZ, given at the dosage of
201 500 mg twice a day for 5 days, was used to treat 150 severe COVID-19 patients in a
202 public hospital in Guayaquil, Ecuador (Villacís-Bermeo BA, Personal Communication,
203 May 15, 2020). Besides antiviral activity, NTZ is reported to reduce plasma IL-6 level in

204 mice (*41*), which suggests that it also might reduce inflammatory responses. We propose
205 that studies are needed to determine possible combinatorial efficacy of these antivirals in
206 combination with remdesivir in COVID-19 patients.
207

208 **MATERIALS AND METHODS**

209 **Reagents, cells, and viruses**

210 **Reagents:** NTZ used in *in vitro* assays (N0290, Sigma-Aldrich, > 98% purity), JIB-04 E-
211 isomer used in *in vitro* assays (S7281, Selleckchem, 99.8% purity), JIB-04 E-isomer used
212 in *in vivo* experiments (HY-13953, Med-ChemExpress), Fluvoxamine maleate (S1336,
213 Selleckchem), Fluoxetine HCl (S1333, Selleckchem), low molecular weight poly(I:C)
214 complexed with LyoVec (tlrl-picwlv, InvivoGen). EGFP-LC3 plasmid was a gift from
215 Christina Stallings at Washington University School of Medicine. SARS-CoV-2 S plasmid
216 was used as previously described (*42*). pUC19 empty plasmid was used as mock in all
217 transfection experiments.
218

219 **Cells:** Vero E6 cells (CRL-1586, ATCC) and Vero cells (CCL81, ATCC) were cultured in
220 DMEM supplemented with 10% fetal bovine serum (FBS), 10 mM HEPES, 1 mM sodium
221 pyruvate, 0.1 mM non-essential amino acids, and 1 X Penicillin-Streptomycin-
222 Glutamine. Calu-3 cells (HTB-55, ATCC) and swine ST cells (CRL-1746, ATCC) were
223 DMEM supplemented with 10% FBS and 1 X Penicillin-Streptomycin-Glutamine. HEK293,
224 HEK293-hACE2, and HEK293-hACE2-TMPRSS2 cells were cultured in complete DMEM
225 containing G418 and/or blasticidin and used as previously described (*11*). MA104 and
226 Vero E6-TMPRSS2 cells were cultured as before (*42*).

227

228 **Viruses:** Rhesus RV RRV strain, bovine RV UK strain, and porcine RV NJ2012 strain
229 (Genbank: MT874983-MT874993) were propagated and titrated as before (*43*). Vaccinia
230 virus MVA strain was used as before (*44*). HSV-1 syn17+ strain was a gift from Ann Arvin
231 at Stanford University. TGEV JS2012 strain was propagated as before (*45*). TGEV was
232 titrated by serial dilutions in cells in 96-well plates that were seeded at a density of 1 X
233 10^4 cells per well. Cytopathic effects were observed at 3-7 dpi and the $TCID_{50}$ values
234 were calculated and converted to PFU/ml. A clinical isolate of SARS-CoV-2 (2019-
235 nCoV/USA-WA1/2020 strain) was obtained from the Centers for Disease Control and
236 Prevention (gift of Natalie Thornburg). A SARS-CoV-2 mNeonGreen reporter virus was
237 used as previously reported (*18*). Both the clinical isolate and the mNeonGreen SARS-
238 CoV-2 viruses were propagated in Vero CCL81 cells and titrated by focus-forming assays
239 on Vero E6 cells. Recombinant VSV-eGFP (*22*) and VSV-eGFP-SARS-CoV-2 were
240 previously described (*23*). Cells infected with GFP-positive virus were imaged with ECHO
241 REVOLVE 4 fluorescence microscope. Plaque assays were performed in MA104 cells
242 seeded in 6-well plates using an adapted version of the rotavirus plaque assay protocol
243 (*43*).

244

245 **Inhibitor screen**

246 The small-molecule inhibitors used in this study are from in-house collection and the
247 COVID Box (Medicines for Malaria Venture; www.mmv.org/mmv-open/covid-box).
248 Compound names, vendors, and catalog numbers are listed in **Table S1**. At 24 hpi, cells
249 were fixed in 4% paraformaldehyde (PFA) in PBS and stained with Hoechst 33342. The

250 levels of viral antigens, reflected by mNeonGreen signals, were scanned by Amersham
251 Typhoon 5 (GE). Image background was subtracted using rolling ball algorithm (radius =
252 5 pixels). To further remove the imaging artifacts and well-to-well variation, we removed
253 the region which fell below the threshold calculated by Moments algorithm. Number of
254 positive pixels and total intensity (after background subtraction) were computed for each
255 well and log10 transformed. The number of cells in each well was quantified based on
256 Hoechst 33342 staining detected by Cytation 3 imaging reader (BioTek). Image analysis
257 was performed using ImageJ and customized R scripts. The quantification of
258 mNeonGreen and Hoechst 33342 is provided in **Dataset S1**.
259

260 **Cell cytotoxicity assay**

261 The viability of Vero E6 and MA104 cells after drug treatment was determined using the
262 Cell Counting Kit 8 (ab228554, Abcam). Briefly, cells in 96-well plates were treated with
263 NTZ or JIB-04 at desired concentrations at 37°C. After 25 hr of incubation, the inhibitor-
264 containing medium was replaced with fresh complete medium with 10 μl of WST-8
265 solution in each well. The cells were incubated at 37 °C for 2 hr with protection from light.
266 Absorbance at 460nm was measured using Gen5 software and BioTek ELx800
267 Microplate Reader.
268

269 **RNA extraction and quantitative PCR**

270 Total RNA was extracted from cells using RNeasy Mini kit (Qiagen). For spike plasmid
271 transfection experiments, total RNA was extracted using Aurum Total RNA Mini Kit
272 (Biorad) with DNase digestion. Complementary DNA was synthesized with High Capacity

273 cDNA Reverse Transcription kit (Thermo Fisher) as previously described (*46*).
274 Quantitative PCR was performed using AriaMX (Agilent) with 12.5 µl of either Power
275 SYBR Green master mix or Taqman master mix (Applied Biosystems) in a 25 µl reaction.
276 Gene expression was normalized to the housekeeping gene GAPDH. All SYBR Green
277 primers and Taqman probes used in this study are listed in **Table S2**.
278
279 **Western blotting**
280 Cells were lysed in RIPA buffer supplemented with protease inhibitor cocktail and
281 phosphatase inhibitor. Lysates were boiled for 5 min in 1 x Laemmli Sample Buffer (Bio-
282 Rad) containing 5% β-mercaptoethanol. Proteins were resolved in SDS-PAGE and
283 detected as described (*47*) using the following antibodies: GAPDH (631402, Biolegend),
284 rotavirus VP6 (rabbit polyclonal, ABclonal technology), and SARS-CoV-2 S2 (40592-T62,
285 Sino Biological). Secondary antibodies were anti-rabbit (7074, Cell Signaling) or anti-
286 mouse (7076, Cell Signaling) immunoglobulin G horseradish peroxidase-linked
287 antibodies. Protein bands were visualized with Clarity ECL Substrate (Bio-rad) and a
288 Biorad Gel Doc XR system.
289
290 **Small interfering RNA transfection**
291 HEK293 cells were transfected using Lipofectamine RNAiMAX Transfection Reagent
292 (Thermo Fisher). Cells were harvested at 48 hr post transfection and knockdown
293 efficiency was determined by RT-qPCR. siRNA transfected cells were infected with PoRV
294 (MOI=0.01) for 12 hr and viral RNA copy numbers were examined by RT-qPCR. All siRNA

295 used in this study were designed and synthesized by GenePharma (Shanghai, China)
296 and their sequences of siRNAs are listed in **Table S2**.
297
298 **Flow cytometry**
299 Vero E6-TMPRSS2 cells were inoculated with VSV-GFP or VSV-SARS-CoV-2 at an MOI
300 of 3 for 1 hr at 37°C. At 6 hpi, cells were harvested and fixed in 4% PFA in PBS.
301 Percentage of GFP positive cells and GFP intensity were determined by BD
302 LSRFortessa™ X-20 cell analyzer and analyzed by FlowJo v10.6.2 (BD).
303
304 **RNA-sequencing**
305 HEK293 cells were pre-treated with JIB-04 (10 μM) for 12 hr, and mock or porcine RV-
306 infected (MOI=0.01) for another 12 hr. Total RNA from cells in triplicate was extracted
307 using RNeasy Mini kit (Qiagen). RNA sample quality was measured by both NanoDrop
308 spectrophotometer (Thermo Fisher) and Bioanalyzer 2100 (Agilent). Libraries were
309 sequenced on the Illumina NovaSeq 6000 platform. Differential gene expression analysis
310 was performed using DESeq2. The RNA-seq raw and processed datasets were deposited
311 onto NCBI Gene Expression Omnibus database (GSE156219).
312
313 **TGEV piglet infection**
314 Newborn piglets (Landrace × Yorkshire) were spontaneously delivered from sows, and
315 their body weights were recorded at birth. Fifteen neonatal male pigs at birth were
316 obtained from a TGEV-free farm in Nanjing without suckling. All piglets were confirmed
317 negative for TGEV by RT-PCR and ELISA (IDEXX, USA). The pigs were randomly

318 separated into three groups, housed in separate rooms, and fed the same artificial milk
319 substitutes that meet the nutrient and energy recommendations of the National Research
320 Council [NRC, 2012] at the animal facility of the Institute of Veterinary Medicine, Jiangsu
321 Academy of Agricultural Sciences, Nanjing, Jiangsu Province. The experiments were
322 divided into three groups: a DMSO inoculation control group (control, n=5); a DMSO
323 inoculation and TGEV infection group (TGEV-DMSO, n=5); a JIB-04 inoculation and
324 TGEV infection group (TGEV-JIB-04, n=5)). Neonatal pigs were intraperitoneally injected
325 twice with JIB-04 (75 mg/kg) or DMSO at 24 hr and 6 hr prior to TGEV infection. TGEV-
326 DMSO and TGEV-JIB-04 groups were orally infected with $1\times10^{7.25}$ (1.778×10^{7}) $TCID_{50}$
327 (equivalent to 1.245×10^{7} PFU) of TGEV in 1.5 ml of DMEM per pig. Neonatal pigs were
328 weighed and observed for clinical signs every 8 hr throughout the study. Serum samples
329 were collected from each pig at 24 and 48 hpi to detect specific anti-TGEV antibodies.
330 The occurrence of diarrhea was monitored, and its severity was recorded based on an
331 established scoring system (*44*). In brief, diarrhea was scored on the basis of color,
332 consistency, and amount, and numbered as follows: 0 = normal; 1 = pasty; 2 = semi-liquid;
333 3 = liquid, and score ≥ 2 considered as diarrhea. At 48 hpi, all pigs were euthanized, and
334 intestinal tissues were collected for pathological examination and viral load analysis using
335 RT-qPCR and primers in **Table S2**.
336

337 **Histopathological and immunofluorescence analysis**

338 Intestinal tissues harvested from pigs were fixed in 4% PFA in PBS and incubated in 50%
339 ethanol overnight. After fixation, tissues were embedded in paraffin, sectioned, and
340 subjected to hematoxylin and eosin staining by standard procedures. For

341 immunofluorescence analysis, samples were incubated with rabbit anti-TGEV-N antibody
342 (1:500, DA0224, Shanghai YouLong Biotech) for 30 min at 37 ºC. After three washes,
343 samples were stained with Cy3-conjugated goat anti-rabbit secondary antibody
344 (Beyotime) and DAPI (Invitrogen). Images were obtained using a fluorescence
345 microscope (Carl Zeiss).
346
347 **Ethics statement**
348 Animal experiments were approved by the Committee on the Ethics of Animal Care and
349 Use of the Science and Technology Agency of Jiangsu Province. The approval ID is
350 NKYVET 2014-63, granted by the Jiangsu Academy of Agricultural Sciences
351 Experimental Animal Ethics Committee. All efforts were made to minimize animal
352 suffering. The virus challenge and tissue collection were performed in strict accordance
353 with the guidelines of Jiangsu Province Animal Regulations (Decree No. 2020-18).
354
355 **Statistical analysis**
356 All bar graphs were displayed as means ± standard error of mean (SEM). Statistical
357 significance in data Fig. 2E, 2F, 3C, S3D, S3F, 4C, and 4D was calculated by Student's *t*
358 test using Prism 8.4.3 (GraphPad). Statistical significance in data Fig. 1C, 2D, 2G, 3B,
359 3E, 3G, S3A, S3C, and S4B was calculated by pairwise ANOVA using Prism 8.4.3. Non-
360 linear regression (curve fit) was performed to calculate EC_{50} and CC_{50} values for Fig. 1B,
361 2A, and 2C using Prism 8.4.3. HSA synergy model was used to calculate the synergy
362 scores of dose-response data in Fig. 3A. Gehan-Breslow-Wilcoxon test was used to
363 compare the survival curves in Fig. 4B. All data were presented as asterisks (*$p \leq 0.05$;

364 **p≤0.01; ***p≤0.001). All experiments other than Fig. 1A, 3I, and 4 were repeated at least

365 twice. The raw data and p value calculations are included in Dataset S1.

366

367 **SUPPLEMENTARY MATERIALS**

368 Table S1. List of chemicals used in the anti-SARS-CoV-2 compound screen

369 Table S2. List of quantitative PCR primers and siRNA

370 Table S3. Raw data and statistics

371

372

373 **Main Figures and Legends**

374

Figure 1

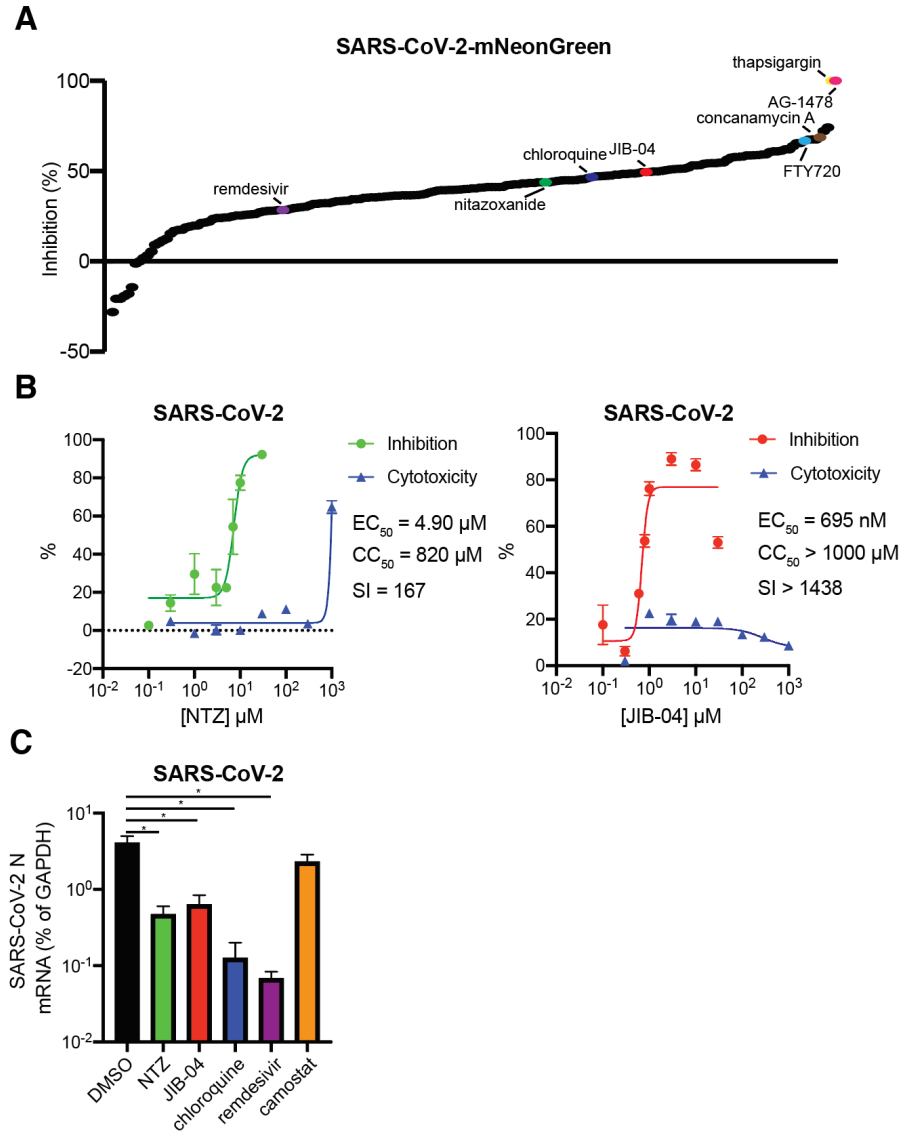

375

376

377 **Fig. 1. Nitazoxanide and JIB-04 inhibit SARS-CoV-2 replication**

378 (A) Small molecule inhibitor screen. Vero E6 cells were treated with individual

379 compounds (listed in Table S1) at 10 μM for 1 hour (hr) and infected with SARS-

380 CoV-2-mNeonGreen (MOI=0.5). At 24 hr post infection (hpi), cells were fixed and

381 nuclei were stained by Hoechst 33342. The intensities of mNeonGreen and

382 Hoechst were quantified by the Typhoon biomolecular imager and Cytation plate
383 reader, respectively. The ratio of mNeonGreen and Hoechst is plotted as
384 percentage of inhibition.

385 (B) Dose-response analysis of wild-type SARS-CoV-2 replication with NTZ or JIB-04
386 treatment. Vero E6 cells were treated with compounds for 1 hr and infected with a
387 clinical isolate of SARS-CoV-2 (MOI=0.5). S protein levels were quantified at 24
388 hpi based on immunofluorescence. For CC_{50} measurement, cells were treated with
389 inhibitors at 0.3 μM to 1 mM for 25 hr. SI: selectivity index.

390 (C) Dose-response analysis of intracellular viral RNA levels with compounds. Vero E6
391 cells were treated with NTZ (10 μM), JIB-04 (10 μM), chloroquine (10 μM),
392 remdesivir (3 μM), or camostat (10 μM) for 1 hr and infected with a clinical isolate
393 of SARS-CoV-2 (MOI=0.5). SARS-CoV-2 RNA levels at 24 hpi were measured by
394 RT-qPCR.

395 For all panels except A, experiments were repeated at least three times with similar
396 results. Fig. 1A was performed once with raw data included in Dataset S1. Data
397 are represented as mean ± SEM. Statistical significance is from pooled data of the
398 multiple independent experiments (*$p \leq 0.05$).

399

Figure 2

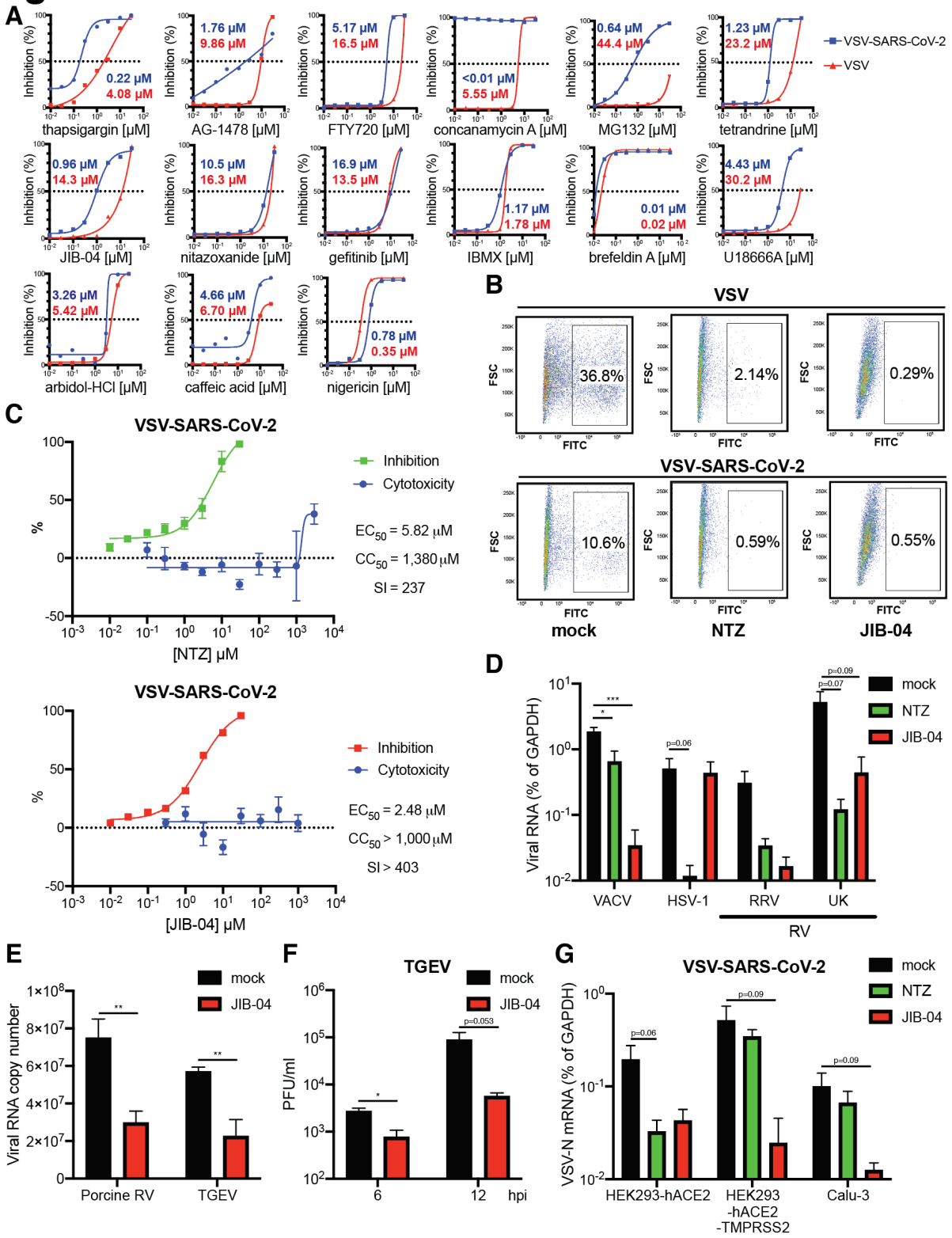
A
Inhibition (%)
0.22 µM
4.08 µM
thapsigargin [µM]
1.76 µM
9.86 µM
AG-1478 [µM]
5.17 µM
16.5 µM
FTY720 [µM]
<0.01 µM
5.55 µM
concanamycin A [µM]
0.64 µM
44.4 µM
MG132 [µM]
1.23 µM
23.2 µM
tetrandrine [µM]
VSV-SARS-CoV-2
VSV
0.96 µM
14.3 µM
JIB-04 [µM]
10.5 µM
16.3 µM
nitazoxanide [µM]
16.9 µM
13.5 µM
gefitinib [µM]
1.17 µM
1.78 µM
IBMX [µM]
0.01 µM
0.02 µM
brefeldin A [µM]
4.43 µM
30.2 µM
U18666A [µM]
3.26 µM
5.42 µM
arbidol-HCl [µM]
4.66 µM
6.70 µM
caffeic acid [µM]
0.78 µM
0.35 µM
nigericin [µM]
B
VSV
FSC
FITC
36.8%
2.14%
0.29%
VSV-SARS-CoV-2
10.6%
0.59%
0.55%
mock
NTZ
JIB-04
C
VSV-SARS-CoV-2
%
Inhibition
Cytotoxicity
EC50 = 5.82 µM
CC50 = 1,380 µM
SI = 237
[NTZ] µM
VSV-SARS-CoV-2
Inhibition
Cytotoxicity
EC50 = 2.48 µM
CC50 > 1,000 µM
SI > 403
[JIB-04] µM
D
Viral RNA (% of GAPDH)
mock
NTZ
JIB-04
p=0.09
p=0.07
p=0.06
VACV
HSV-1
RRV
UK
RV
E
Viral RNA copy number
mock
JIB-04
Porcine RV
TGEV
F
TGEV
PFU/ml
p=0.053
6
12
hpi
G
VSV-SARS-CoV-2
VSV-N mRNA (% of GAPDH)
p=0.06
p=0.09
HEK293-hACE2
HEK293 -hACE2 -TMPRSS2
Calu-3

402 **Fig. 2. Nitazoxanide and JIB-04 broadly inhibit DNA and RNA viruses in different**
403 **cell types**

404 (A) Dose-response analysis of VSV and VSV-SARS-CoV-2 replication with 15
405 compounds. MA104 cells were treated with indicated compounds at 0.01 to 30 μM
406 for 1 hr and infected with VSV or VSV-SARS-CoV-2 (MOI=3). GFP signals at 24
407 hpi were quantified to calculate the percentage of inhibition. EC_{50} values for VSV
408 and VSV-SARS-CoV-2 are shown in each graph in red and blue, respectively.

409 (B) Virus infectivity with NTZ or JIB-04 treatment. Vero E6-TMPRSS2 cells were
410 treated with compounds (10 μM) for 1 hr and infected with VSV or VSV-SARS-
411 CoV-2 (MOI=3). At 6 hpi, percentages of GFP positive cells were quantified by flow
412 cytometry.

413 (C) Dose-response analysis of VSV-SARS-CoV-2 replication and cytotoxicity with
414 NTZ or JIB-04 treatment. For EC_{50} measurement, MA104 cells were treated with
415 compounds at 0.01 to 30 μM for 1 hr and infected with VSV-SARS-CoV-2 (MOI=3)
416 for 24 hr. For CC_{50} measurement, cells were treated with compounds at 0.1 μM to
417 3 mM for 25 hr. SI: selectivity index.

418 (D) Intracellular viral RNA levels with NTZ or JIB-04 treatment. MA104 cells were
419 treated with compounds (10 μM) for 1 hr and infected with vaccinia virus (VACV),
420 herpes simplex virus-1 (HSV-1), or rotavirus (RV, RRV and UK strains) (MOI=1).
421 Viral RNA levels at 24 hpi were measured by RT-qPCR for VACV B10R, HSV-1
422 ICP-27, and RV NSP5, respectively.

423 (E) Viral RNA copy numbers with JIB-04 treatment. HEK293 cells were treated with
424 JIB-04 (10 μM) for 6 hr and infected with porcine rotavirus (MOI=0.01) for 6 hr. ST

425 cells were treated with JIB-04 (10 μM) for 12 hr and infected with transmissible
426 gastroenteritis virus (TGEV) (MOI=0.01) for 12 hr. Viral RNA copy numbers were
427 measured by RT-qPCR.
428 (F) TGEV titers in the cell supernatant with JIB-04 treatment. ST cells were treated
429 with JIB-04 (10 μM) for 12 hr and infected with TGEV (MOI=0.01). Virus titers at 6
430 and 12 hpi were measured by plaque assays.
431 (G) Intracellular viral RNA levels with NTZ or JIB-04 treatment in different cell types.
432 HEK293-hACE2, HEK293-hACE2-TMPRSS2, and Calu-3 cells were treated with
433 compounds (10 μM) for 1 hr and infected with VSV-SARS-CoV-2 (MOI=1). VSV
434 RNA levels at 24 hpi were measured by RT-qPCR.
435 For all panels except A, experiments were repeated at least three times with similar
436 results. Fig. 2A was performed once. Data are represented as mean ± SEM.
437 Statistical significance is from pooled data of the multiple independent experiments
438 (*$p \leq 0.05$; **$p \leq 0.01$; ***$p \leq 0.001$).
439

Figure 3

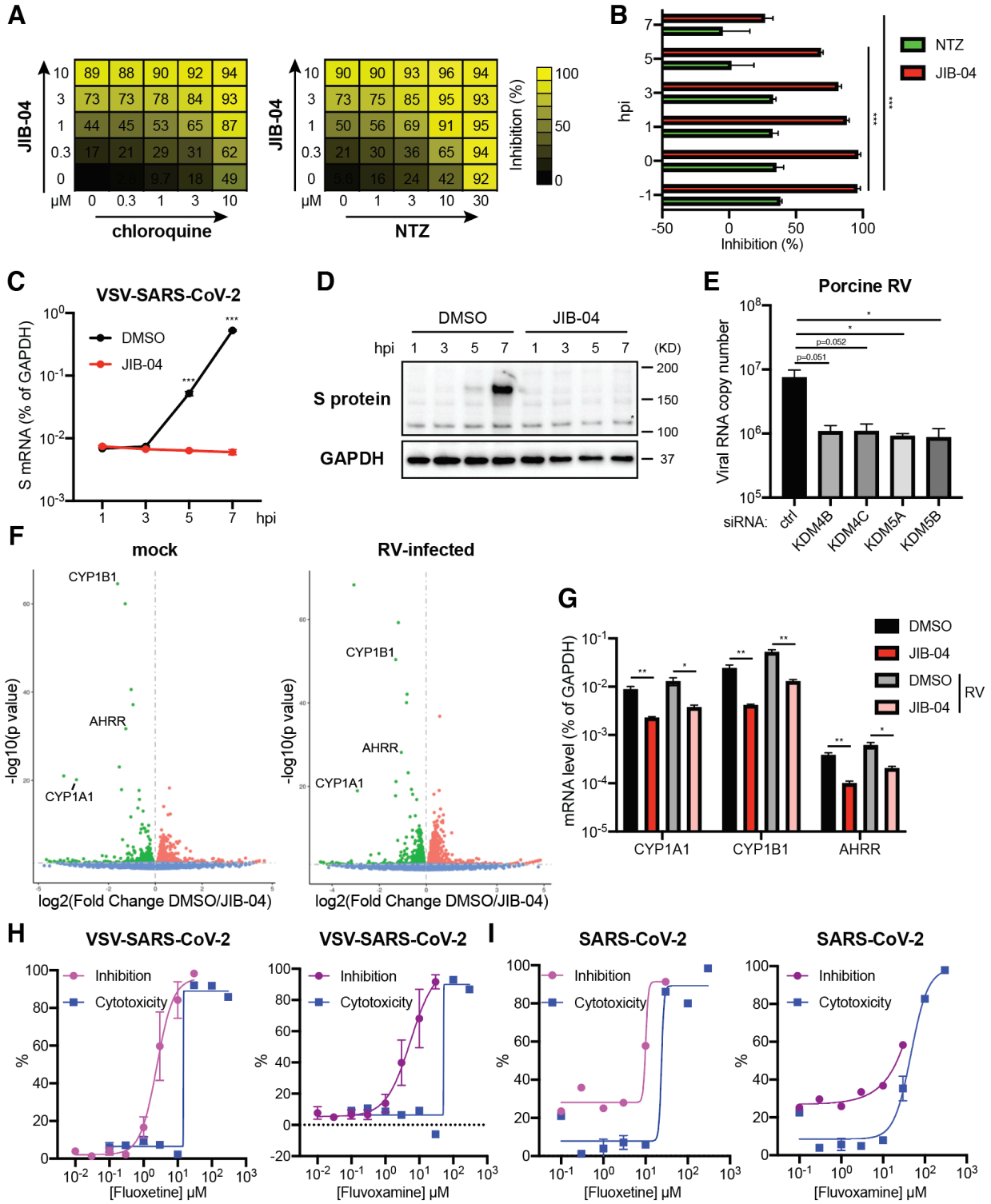
A
JIB-04
10 89 88 90 92 94
3 73 73 78 84 93
1 44 45 53 65 87
0.3 17 21 29 31 62
0 9.7 18 49
μM 0 0.3 1 3 10
chloroquine
10 90 90 93 96 94
3 73 75 85 95 93
1 50 56 69 91 95
0.3 21 30 36 65 94
0 5.6 16 24 42 92
μM 0 1 3 10 30
NTZ
Inhibition (%)
100
50
0
B
hpi
7
5
3
1
0
-1
-50 0 50 100
Inhibition (%)
NTZ
JIB-04
C
VSV-SARS-CoV-2
S mRNA (% of GAPDH)
DMSO
JIB-04
hpi
D
DMSO
JIB-04
hpi 1 3 5 7 1 3 5 7 (KD)
S protein
GAPDH
200
150
100
37
E
Porcine RV
Viral RNA copy number
p=0.051
p=0.052
siRNA: ctrl KDM4B KDM4C KDM5A KDM5B
F
mock
RV-infected
CYP1B1
AHRR
CYP1A1
-log10(p value)
log2(Fold Change DMSO/JIB-04)
G
mRNA level (% of GAPDH)
DMSO
JIB-04
DMSO
JIB-04
RV
CYP1A1
CYP1B1
AHRR
H
VSV-SARS-CoV-2
Inhibition
Cytotoxicity
%
[Fluoxetine] μM
[Fluvoxamine] μM
I
SARS-CoV-2
Inhibition
Cytotoxicity
%
[Fluoxetine] μM
[Fluvoxamine] μM

442 **Fig. 3. JIB-04 exhibits distinct post-entry antiviral mechanisms**

443 (A) Drug combination dose-response matrix and VSV-SARS-CoV-2 replication.
444 MA104 cells were treated with JIB-04 and chloroquine or JIB-04 and NTZ for 1 hr
445 and infected with VSV-SARS-CoV-2 (MOI=3). GFP signals at 24 hpi were
446 quantified to calculate the percentage of inhibition.

447 (B) Time of compound addition and VSV-SARS-CoV-2 replication. MA104 cells were
448 treated with NTZ or JIB-04 (10 μM) at indicated time points relative to VSV-SARS-
449 CoV-2 infection (MOI=3, 0 hpi). GFP signals at 8 hpi were quantified to calculate
450 the percentage of inhibition.

451 (C) Intracellular SARS-CoV-2 S RNA levels with JIB-04 treatment. MA104 cells were
452 treated with JIB-04 (10 μM) for 1 hr and infected with VSV-SARS-CoV-2 (MOI=1)
453 for 1, 3, 5, and 7 hr. S RNA levels were measured by RT-qPCR.

454 (D) Western blot analysis of SARS-CoV-2 S protein levels with JIB-04 treatment.
455 MA104 cells were treated with JIB-04 (10 μM) for 1 hr and infected with VSV-
456 SARS-CoV-2 (MOI=1) for 1, 3, 5, and 7 hr. FL: full-length. S2: cleaved S2 fragment.
457 (* non-specific band)

458 (E) Histone demethylase siRNA knockdown and RV replication. HEK293 cells were
459 transfected with scrambled siRNA or siRNA targeting indicated histone
460 demethylases for 48 hr and infected with porcine RV (MOI=0.01). Viral RNA copy
461 numbers at 12 hpi were quantified by RT-qPCR.

462 (F) Volcano plot of differentially expressed transcripts with JIB-04 treatment and RV
463 infection. HEK293 cells were treated with DMSO or JIB-04 (10 μM) for 12 hr, and
464 mock-infected (left panel) or infected with porcine RV (MOI=0.01, right panel) for

465 another 12 hr. Red dots represent upregulated genes and green dots represent
466 downregulated genes in JIB-04 treated cells.
467 (G) Expression of three top genes in (F) with JIB-04 treatment. HEK293 cells were
468 treated with JIB-04 (10 μM) for 12 hr and mock-infected or infected porcine RV
469 (MOI=0.01) for 12 hr. mRNA levels of CYP1A1, CYP1B1, and AHRR at 12 hpi
470 were measured by RT-qPCR.
471 (H) Dose-response analysis of VSV-SARS-CoV-2 replication with fluoxetine or
472 fluvoxamine treatment. MA104 cells were treated with compounds at 0.01 to 30
473 μM for 1 hr and infected with VSV-SARS-CoV-2 (MOI=3). GFP signals at 24 hpi
474 were quantified to calculate the percentage of inhibition. For CC_{50} measurement,
475 cells were treated with compounds at 0.1 μM to 300 μM for 25 hr.
476 (I) Dose-response analysis of wild-type SARS-CoV-2 replication with fluoxetine or
477 fluvoxamine treatment. Vero E6 cells were treated with compounds for 1 hr and
478 infected with a clinical isolate of SARS-CoV-2 (MOI=0.5). S protein levels at 24 hpi
479 were quantified based on immunofluorescence. For CC_{50} measurement, cells were
480 treated with compounds at 0.1 μM to 300 μM for 25 hr.
481 For all panels except A and I, experiments were repeated at least three times with
482 similar results. Fig. 3A was performed twice. Inhibition assay in Fig. 3I was
483 performed once and cytotoxicity assay was performed in triplicates. Data are
484 represented as mean ± SEM. Statistical significance is from pooled data of the
485 multiple independent experiments (*$p \leq 0.05$; **$p \leq 0.01$; ***$p \leq 0.001$).
486

Figure 4

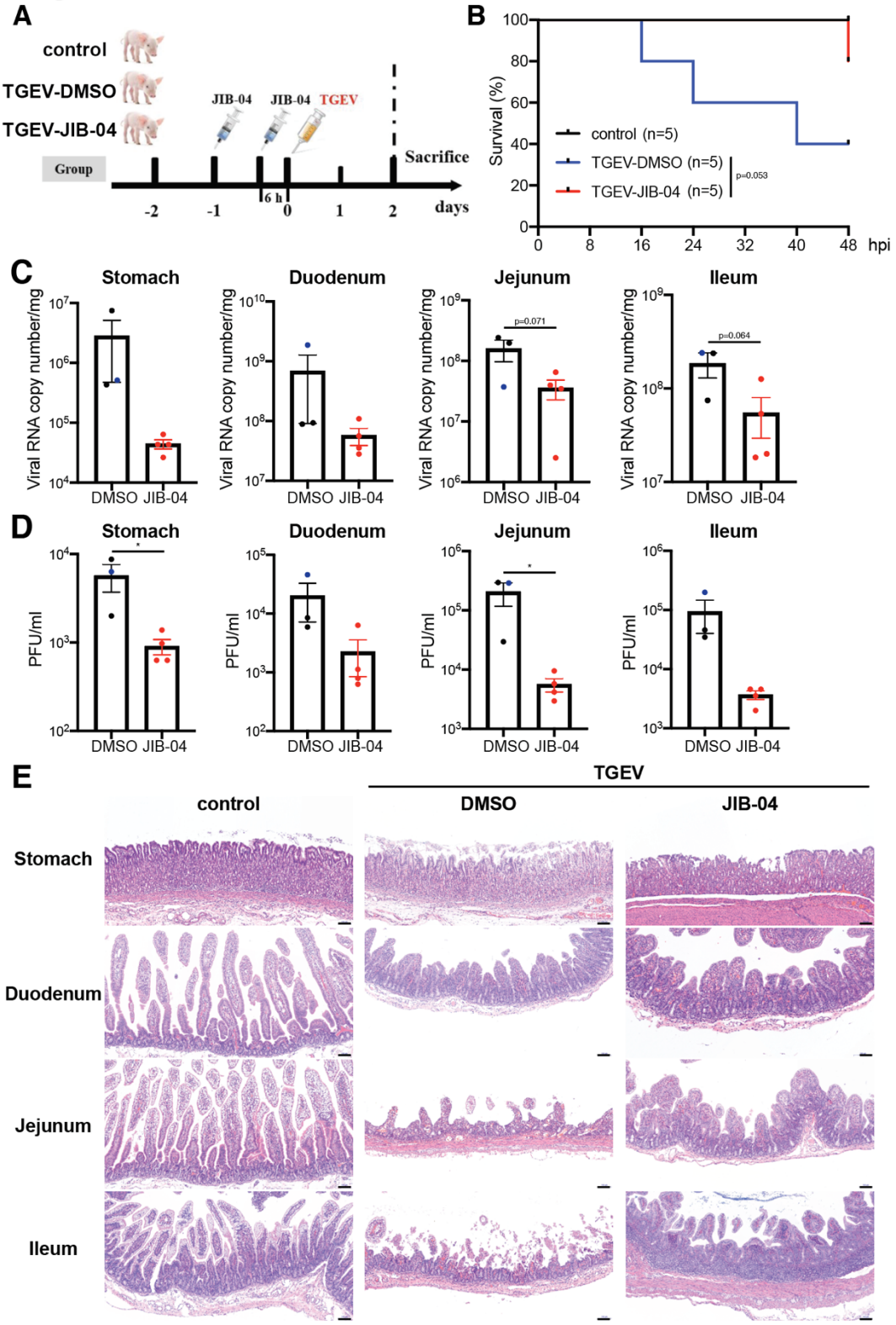

Fig. 4. JIB-04 suppresses TGEV replication and pathogenesis in pigs

490 (A) Experimental schemes for testing the protective efficacy of JIB-04 treatment
491 against TGEV challenge in three groups of neonatal pigs. Control: DMSO injection,
492 mock infection; TGEV-DMSO: DMSO injection, TGEV infection; TGEV-JIB-04:
493 JIB-04 injection, TGEV infection.
494 (B) Survival curve of TGEV infected pigs with JIB-04 treatment. Neonatal pigs were
495 intraperitoneally injected with vehicle control DMSO or JIB-04 and mock-infected
496 or infected with 1.2×10^7 PFU of TGEV. Survival was monitored every 8 hr with
497 data censored at 48 hpi, when all pigs were sacrificed.
498 (C) TGEV RNA copy numbers in the gastrointestinal (GI) tract of infected pigs. TGEV
499 infected piglets were sacrificed at 48 hpi. For the DMSO group, two animals
500 sacrificed at 48 hpi and one that died at 40 hpi (colored in blue) were examined.
501 For the JIB-04 groups, four animals sacrificed at 48 hpi were examined. TGEV
502 genome copy numbers at 48 hpi were quantified by RT-qPCR.
503 (D) Same as (C) except that virus titers were measured by plaque assays.
504 (E) Hematoxylin and eosin staining of different GI tract sections from pigs sacrificed at
505 48 hpi. Representative images of 3 animals. Scale bar, 100 μm.
506 Data are represented as mean ± SEM. Statistical significance is from pooled data
507 of the multiple independent experiments (*$p \leq 0.05$).
508

509 **Supplemental Figures and Legends**

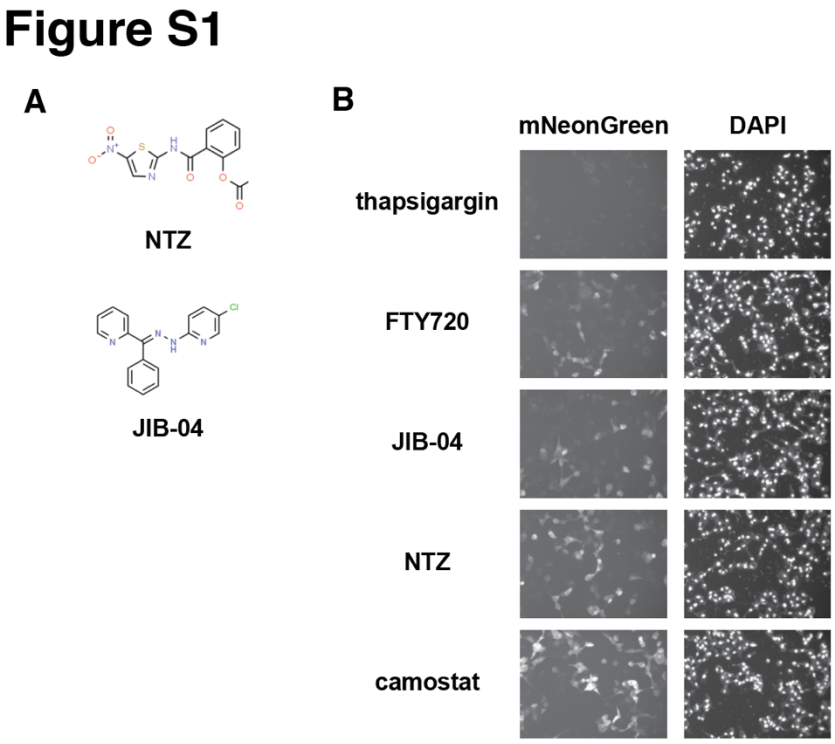

510
511
512 **Fig. S1. Nitazoxanide and JIB-04 inhibit SARS-CoV-2 replication**

513 (A) Chemical structures of NTZ and JIB-04 E-isomer from ChemSpider database.

514 (B) Representative images of Vero E6 cells infected by SARS-CoV-2-mNeonGreen

515 (MOI=0.5) at 24 hpi in Fig. 1A.

516 Experiments were repeated at least three times with similar results.

517

518

Figure S2

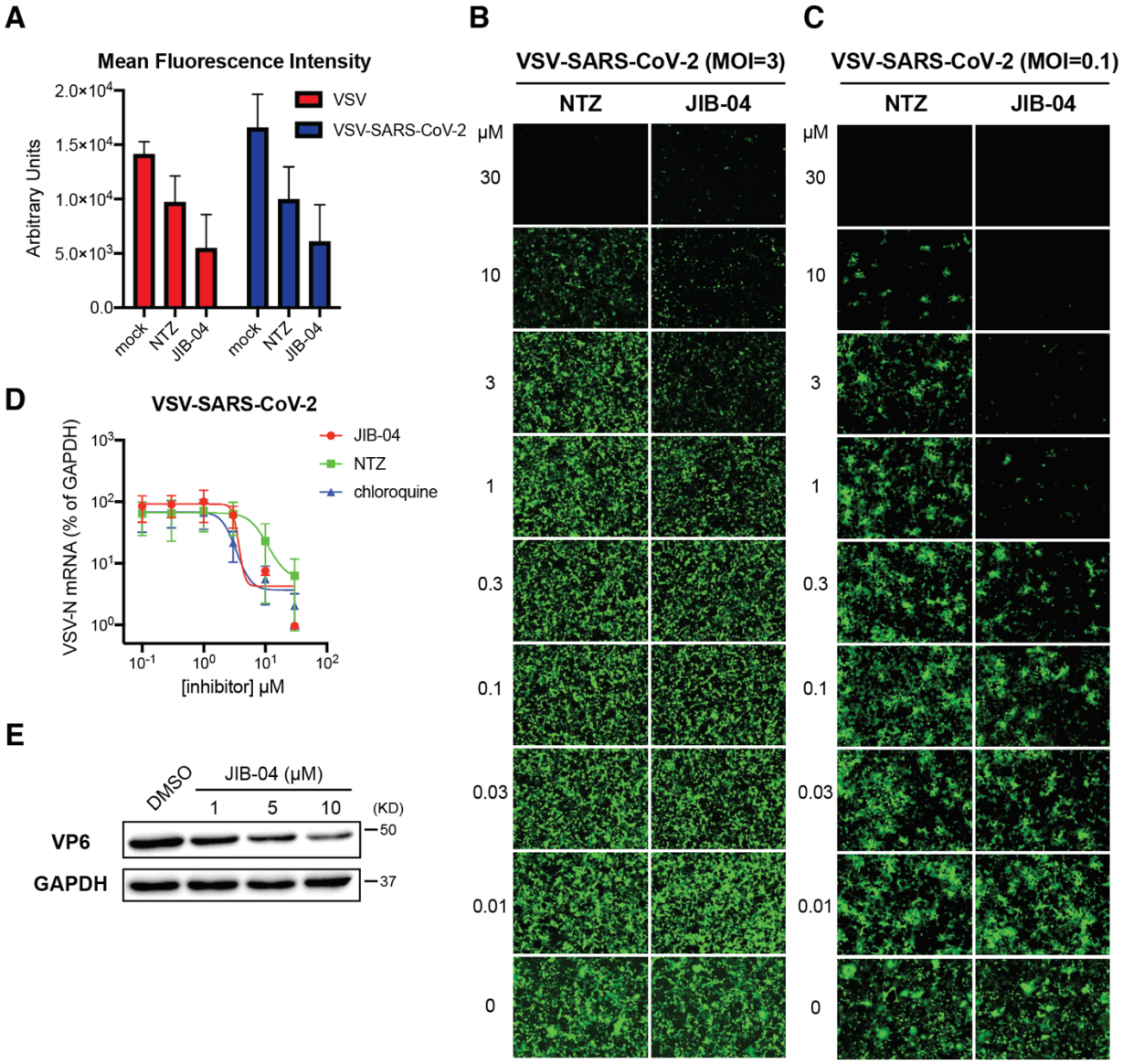

Fig. S2. Nitazoxanide and JIB-04 inhibit the replication of multiple viruses

(A) Mean fluorescence intensity of GFP positive cells in Fig. 2B was quantified by flow cytometry.

524 (B) Dose-response analysis of VSV-SARS-CoV-2 replication with NTZ or JIB-04
525 treatment. MA104 cells were treated with compounds at indicated concentrations
526 for 1 hr and infected with VSV-SARS-CoV-2 (MOI=3). At 24 hpi, images of GFP
527 positive infected cells were acquired by the ECHO fluorescence microscope.
528 (C) Same as (B) except that cells were infected with an MOI of 0.1.
529 (D) Dose-response analysis of intracellular viral RNA levels with NTZ, JIB-04, or
530 chloroquine treatment. MA104 cells were treated with compounds at 0.1 to 30 μM
531 for 1 hr and infected with VSV-SARS-CoV-2 (MOI=3). VSV RNA levels at 24 hpi
532 were measured by RT-qPCR.
533 (E) Western blot analysis of RV antigen VP6 levels with JIB-04 treatment. HEK293
534 cells were treated with JIB-04 at 1, 5, or 10 μM for 6 hr and infected with porcine
535 RV (MOI=0.01) for 12 hr. GAPDH was used as a loading control.
536 All experiments were repeated at least three times with similar results. Data are
537 represented as mean ± SEM.
538
539
540

Figure S3

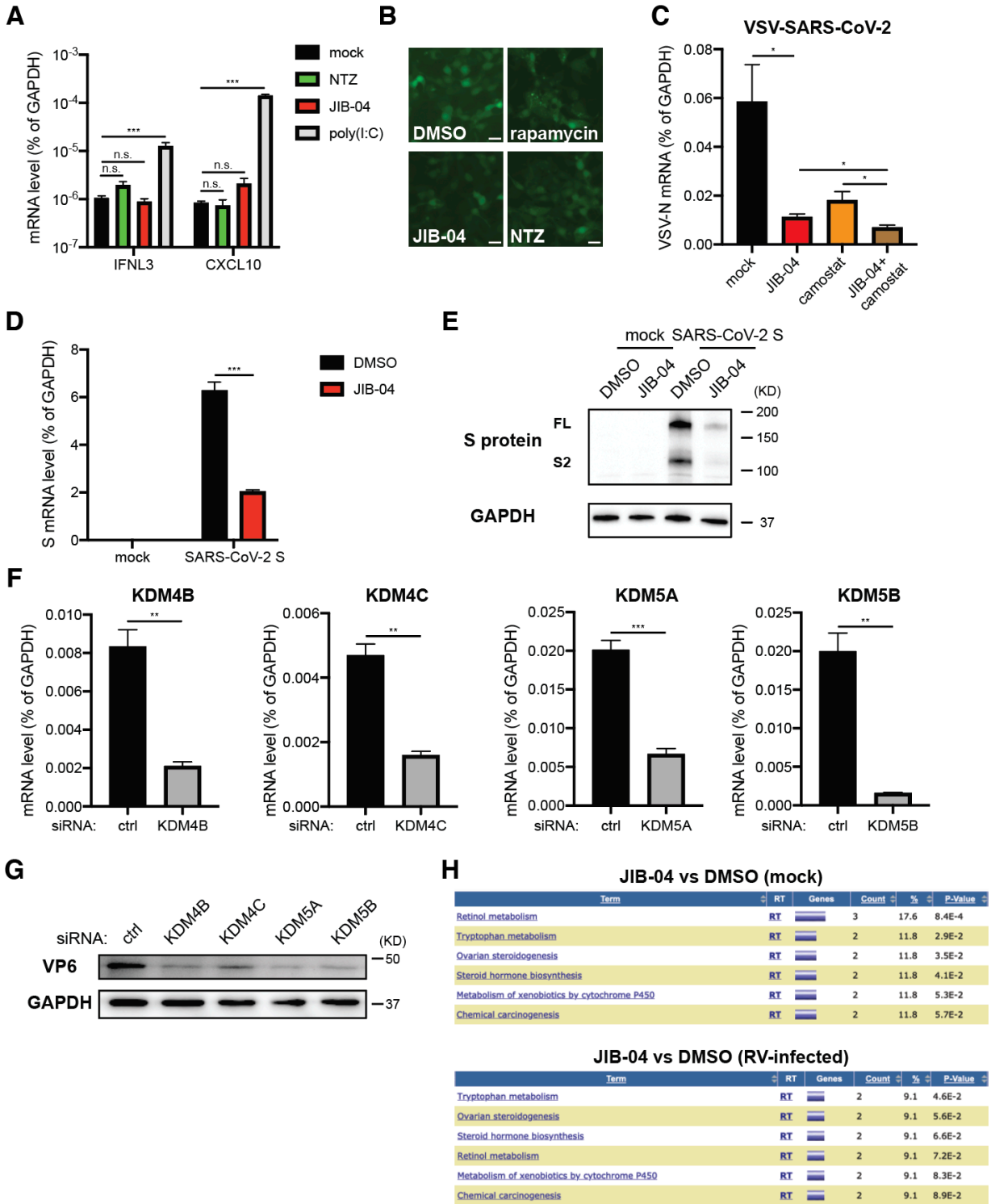

Term	RT	Genes	Count	%	P-Value
Retinol metabolism	RT		3	17.6	8.4E-4
Tryptophan metabolism	RT		2	11.8	2.9E-2
Ovarian steroidogenesis	RT		2	11.8	3.5E-2
Steroid hormone biosynthesis	RT		2	11.8	4.1E-2
Metabolism of xenobiotics by cytochrome P450	RT		2	11.8	5.3E-2
Chemical carcinogenesis	RT		2	11.8	5.7E-2

Term	RT	Genes	Count	%	P-Value
Tryptophan metabolism	RT		2	9.1	4.6E-2
Ovarian steroidogenesis	RT		2	9.1	5.6E-2
Steroid hormone biosynthesis	RT		2	9.1	6.6E-2
Retinol metabolism	RT		2	9.1	7.2E-2
Metabolism of xenobiotics by cytochrome P450	RT		2	9.1	8.3E-2
Chemical carcinogenesis	RT		2	9.1	8.9E-2

541

542 **Fig. S3. Inhibition or knockdown of specific KDM histone demethylases inhibits**
543 **virus replication**

544 (A) Expression of IFN and IFN-stimulated genes with NTZ or JIB-04 treatment.
545 HEK293 cells were treated with NTZ (10 μM), JIB-04 (3 μM), or transfected with
546 low-molecular-weight poly(I:C) (100 ng/ml) for 24 hr. mRNA levels of IFNL3 and
547 CXCL10 were measured by RT-qPCR.

548 (B) Autophagy formation with compound treatment. HEK293 cells were transfected
549 with EGFP-LC3 plasmid for 24 hr and treated with rapamycin (100 nM), NTZ (10
550 μM), or JIB-04 (3 μM) for another 18 hr. GFP positive punctate structures indicate
551 autophagy activation. Scale bar, 20 μm.

552 (C) Intracellular viral RNA levels with JIB-04 and camostat treatment. Calu-3 cells were
553 treated with compounds (10 μM) for 1 hr and infected with VSV-SARS-CoV
554 (MOI=3). VSV RNA levels at 24 hpi were measured by RT-qPCR.

555 (D) Intracellular SARS-CoV-2 S RNA levels with JIB-04 treatment. HEK293 cells were
556 transfected with SARS-CoV-2 S plasmid for 2 hr and treated with JIB-04 (3 μM) for
557 24 hr. S RNA levels were measured by RT-qPCR.

558 (E) Western blot analysis of SARS-CoV-2 S protein levels with JIB-04 treatment.
559 HEK293 cells were transfected with SARS-CoV-2 S plasmid for 2 hr and treated
560 with JIB-04 (3 μM) for 24 hr. FL: full-length. S2: cleaved S2 fragment.

561 (F) siRNA-mediated knockdown of JIB-04 target histone demethylases. HEK293 cells
562 were transfected with scrambled siRNA or siRNA targeting indicated histone
563 demethylases for 48 hr. mRNA levels of indicated histone demethylases were
564 measured by RT-qPCR.

565 (G) Western blot analysis of RV antigen VP6 levels in cells with histone demethylase
566 siRNA knockdown. HEK293 cells were transfected with scrambled siRNA or siRNA
567 targeting indicated histone demethylases for 48 hr and infected with porcine RV
568 (MOI=0.01) for 12 hr.
569 (H) Pathway enrichment analysis of gene expression regulated by JIB-04 treatment.
570 Downregulated genes in Fig. 3F with p values < 1e-10 were analyzed by DAVID
571 functional annotation.
572 All experiments were repeated at least three times with similar results. Data are
573 represented as mean ± SEM. Statistical significance is from pooled data of the
574 multiple independent experiments (*$p \leq 0.05$; **$p \leq 0.01$; ***$p \leq 0.001$).
575
576

Figure S4

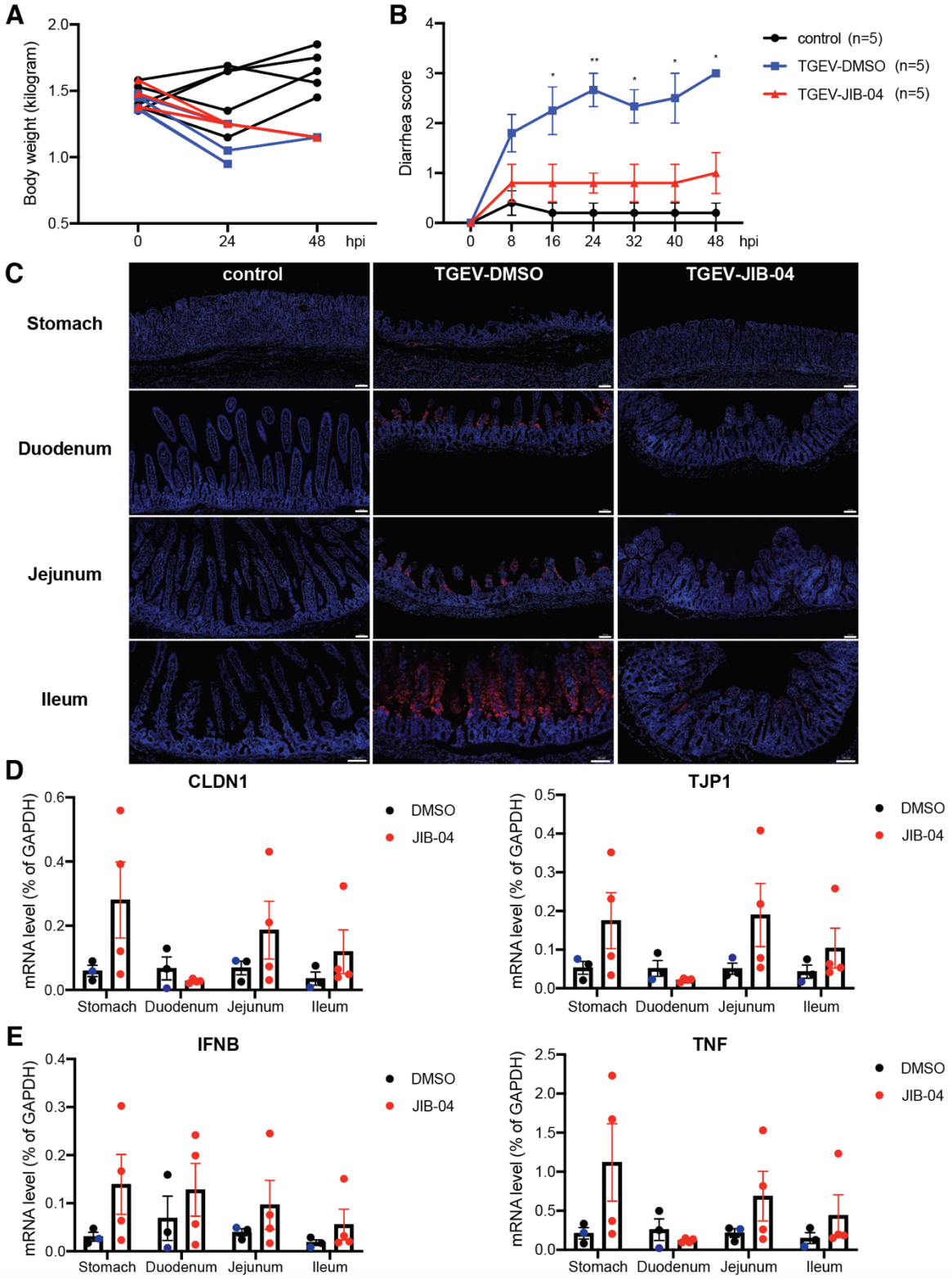

Fig. S4. JIB-04 reduces TGEV induced weight loss and pathogenesis

580 (A) Weight of TGEV infected pigs with JIB-04 treatment in Fig. 4B. The body weight of
581 individual animals was monitored every 24 hr.
582 (B) Diarrhea occurrence in TGEV infected pigs with JIB-04 treatment in Fig. 4B.
583 Diarrhea severity was scored for the fecal specimens of DMSO or JIB-04 treated,
584 mock or TGEV infected animals every 8 hr.
585 (C) Immunofluorescence staining of TGEV antigen in different GI tract sections from
586 pigs sacrificed at 48 hpi. Blue: cell nuclei; red: TGEV nucleocapsid protein.
587 Representative images of 3 animals. Scale bar, 100 μm.
588 (D) Expression of tight junction associated genes in the GI tract of TGEV infected pigs
589 with JIB-04 treatment. For the DMSO group, two animals sacrificed at 48 hpi and
590 one that died at 40 hpi (colored in blue) were examined. For the JIB-04 groups,
591 four animals sacrificed at 48 hpi were examined. CLDN1 and TJP1 mRNA levels
592 at 48 hpi were measured by RT-qPCR.
593 (E) Same as (D) except that IFNB and TNF mRNA levels were measured instead.
594 Data are represented as mean ± SEM. Statistical significance is from pooled data
595 of the multiple independent experiments (*$p \leq 0.05$; **$p \leq 0.01$).
596
597
598
599

REFERENCES AND NOTES

1. F. Touret, Gilles, M., Barral, K., Nougairede, A., Decroly, E., de Lamballerie, X., Coutard, B., In vitro screening of a FDA approved chemical library reveals potential inhibitors of SARS-CoV-2 replication. *bioRxiv*, (2020).
2. L. Riva, Yuan, S., Yin, X., Martin-Sancho, L., Matsunaga, N., et al., , A Large-scale Drug Repositioning Survey for SARS-CoV-2 Antivirals. *bioRxiv*, (2020).
3. C. Mirabelli, Wotring, J.W., Zhang, C.J., McCarty, S.M., Fursmidt, R., et al., , Morphological Cell Profiling of SARS-CoV-2 Infection Identifies Drug Repurposing Candidates for COVID-19. *bioRxiv*, (2020).
4. M. Dittmar, Lee, J.S., Whig, K., Segrist, E., Li, M., Jurado, K., Samby, K., Ramage, H., Schultz, D., Cherry, S., Drug repurposing screens reveal FDA approved drugs active against SARS-Cov-2. *bioRxiv*, (2020).
5. K. Heiser, McLean, P.F., Davis, C.T., et al., , Identification of potential treatments for COVID-19 through artificial intelligence-enabled phenomic analysis of human cells infected with SARS-CoV-2. *bioRxiv*, (2020).
6. F. Wu *et al.*, A new coronavirus associated with human respiratory disease in China. *Nature* **579**, 265-269 (2020).
7. P. Zhou *et al.*, A pneumonia outbreak associated with a new coronavirus of probable bat origin. *Nature* **579**, 270-273 (2020).
8. M. Hoffmann *et al.*, SARS-CoV-2 Cell Entry Depends on ACE2 and TMPRSS2 and Is Blocked by a Clinically Proven Protease Inhibitor. *Cell*, (2020).
9. M. Wang *et al.*, Remdesivir and chloroquine effectively inhibit the recently emerged novel coronavirus (2019-nCoV) in vitro. *Cell research* **30**, 269-271 (2020).
10. Y. L. Kang, Chou, Y.Y., Rothlauf, P.W., Liu, Z., Soh, T.K., Cureton, D., Case, J.B., Chen, R.E., Diamond, M.S., Whelan, S.P.J., Kirchhausen, T., Inhibition of PIKfyve kinase prevents infection by EBOV and SARS-CoV-2. *bioRxiv*, (2020).
11. R. Zang, Case, J.B., Gomez Castro, M.F., Liu, Z., Zeng, Q., Zhao, H., Son, J., Rothlauf, P.W., Hou, G., Bose, S., Wang, X., Vahey, M.D., Kirchhausen, T., Fremond, D.H., Diamond, M.S., Whelan, S.P.J., Ding, S., Cholesterol 25-hydroxylase suppresses SARS-CoV-2 replication by blocking membrane fusion. *bioRxiv*, (2020).
12. W. Yin *et al.*, Structural basis for inhibition of the RNA-dependent RNA polymerase from SARS-CoV-2 by remdesivir. *Science*, (2020).
13. Y. Gao *et al.*, Structure of the RNA-dependent RNA polymerase from COVID-19 virus. *Science* **368**, 779-782 (2020).
14. R. N. Kirchdoerfer, A. B. Ward, Structure of the SARS-CoV nsp12 polymerase bound to nsp7 and nsp8 co-factors. *Nature communications* **10**, 2342 (2019).
15. L. Zhang *et al.*, Crystal structure of SARS-CoV-2 main protease provides a basis for design of improved alpha-ketoamide inhibitors. *Science* **368**, 409-412 (2020).
16. W. Dai *et al.*, Structure-based design of antiviral drug candidates targeting the SARS-CoV-2 main protease. *Science*, (2020).
17. Z. Jin *et al.*, Structure of M(pro) from SARS-CoV-2 and discovery of its inhibitors. *Nature* **582**, 289-293 (2020).
18. X. Xie *et al.*, An Infectious cDNA Clone of SARS-CoV-2. *Cell host & microbe*, (2020).

646 19. L. M. Fox, L. D. Saravolatz, Nitazoxanide: a new thiazolide antiparasitic agent.
647 *Clinical infectious diseases : an official publication of the Infectious Diseases*
648 *Society of America* **40**, 1173-1180 (2005).
649 20. L. Wang *et al.*, A small molecule modulates Jumonji histone demethylase activity
650 and selectively inhibits cancer growth. *Nature communications* **4**, 2035 (2013).
651 21. J. Wei, Alfajaro, M.M., Hanna, R.E., et al., , Genome-wide CRISPR screen reveals
652 host genes that regulate SARS-CoV-2 infection. *bioRxiv*, (2020).
653 22. S. Cherry *et al.*, Genome-wide RNAi screen reveals a specific sensitivity of IRES-
654 containing RNA viruses to host translation inhibition. *Genes & development* **19**,
655 445-452 (2005).
656 23. J. B. Case, Rothlauf, P.W., Chen, R.E., Liu, Z., Zhao, H., Kim, A.S., Bloyet, L.,
657 Zeng, Q., Tahan, S., Droit, L., et al.,, Neutralizing antibody and soluble ACE2
658 inhibition of a replication-competent VSV-SARS-CoV-2 and a clinical isolate of
659 SARS-CoV-2. *Cell host & microbe*, (2020).
660 24. W. Dang *et al.*, Nitazoxanide Inhibits Human Norovirus Replication and Synergizes
661 with Ribavirin by Activation of Cellular Antiviral Response. *Antimicrobial agents*
662 *and chemotherapy* **62**, (2018).
663 25. V. Hargest, B. Sharp, B. Livingston, V. Cortez, S. Schultz-Cherry, Astrovirus
664 Replication Is Inhibited by Nitazoxanide In Vitro and In Vivo. *Journal of virology* **94**,
665 (2020).
666 26. S. La Frazia *et al.*, Thiazolides, a new class of antiviral agents effective against
667 rotavirus infection, target viral morphogenesis, inhibiting viroplasm formation.
668 *Journal of virology* **87**, 11096-11106 (2013).
669 27. M. Elazar *et al.*, The anti-hepatitis C agent nitazoxanide induces phosphorylation
670 of eukaryotic initiation factor 2alpha via protein kinase activated by double-
671 stranded RNA activation. *Gastroenterology* **137**, 1827-1835 (2009).
672 28. L. J. Saif, Animal coronavirus vaccines: lessons for SARS. *Dev Biol (Basel)* **119**,
673 129-140 (2004).
674 29. Y. J. Hou *et al.*, SARS-CoV-2 Reverse Genetics Reveals a Variable Infection
675 Gradient in the Respiratory Tract. *Cell*, (2020).
676 30. T. P. Sheahan *et al.*, An orally bioavailable broad-spectrum antiviral inhibits SARS-
677 CoV-2 in human airway epithelial cell cultures and multiple coronaviruses in mice.
678 *Science translational medicine* **12**, (2020).
679 31. M. Xu *et al.*, SHMT2 and the BRCC36/BRISC deubiquitinase regulate HIV-1 Tat
680 K63-ubiquitylation and destruction by autophagy. *PLoS pathogens* **14**, e1007071
681 (2018).
682 32. K. K. Lam *et al.*, Nitazoxanide stimulates autophagy and inhibits mTORC1
683 signaling and intracellular proliferation of Mycobacterium tuberculosis. *PLoS*
684 *pathogens* **8**, e1002691 (2012).
685 33. A. Ianevski, L. He, T. Aittokallio, J. Tang, SynergyFinder: a web application for
686 analyzing drug combination dose-response matrix data. *Bioinformatics* **36**, 2645
687 (2020).
688 34. S. I. Karchner, D. G. Franks, W. H. Powell, M. E. Hahn, Regulatory interactions
689 among three members of the vertebrate aryl hydrocarbon receptor family: AHR
690 repressor, AHR1, and AHR2. *The Journal of biological chemistry* **277**, 6949-6959
691 (2002).

692 35. A. Hemeryck, F. M. Belpaire, Selective serotonin reuptake inhibitors and
693 cytochrome P-450 mediated drug-drug interactions: an update. *Curr Drug Metab*
694 **3**, 13-37 (2002).
695 36. L. Luo *et al.*, Aminopeptidase N-null neonatal piglets are protected from
696 transmissible gastroenteritis virus but not porcine epidemic diarrhea virus.
697 *Scientific reports* **9**, 13186 (2019).
698 37. X. Ou *et al.*, Characterization of spike glycoprotein of SARS-CoV-2 on virus entry
699 and its immune cross-reactivity with SARS-CoV. *Nature communications* **11**, 1620
700 (2020).
701 38. X. Wang *et al.*, The anti-influenza virus drug, arbidol is an efficient inhibitor of
702 SARS-CoV-2 in vitro. *Cell Discov* **6**, 28 (2020).
703 39. Y. L. Kang *et al.*, Inhibition of PIKfyve kinase prevents infection by EBOV and
704 SARS-CoV-2. *bioRxiv*, (2020).
705 40. J. F. Rossignol, H. Maisonneuve, Nitazoxanide in the treatment of Taenia saginata
706 and Hymenolepis nana infections. *The American journal of tropical medicine and*
707 *hygiene* **33**, 511-512 (1984).
708 41. S. K. Hong *et al.*, Nitazoxanide suppresses IL-6 production in LPS-stimulated
709 mouse macrophages and TG-injected mice. *Int Immunopharmacol* **13**, 23-27
710 (2012).
711 42. R. Zang *et al.*, TMPRSS2 and TMPRSS4 promote SARS-CoV-2 infection of
712 human small intestinal enterocytes. *Sci Immunol* **5**, (2020).
713 43. S. Ding *et al.*, Rotavirus VP3 targets MAVS for degradation to inhibit type III
714 interferon expression in intestinal epithelial cells. *eLife* **7**, (2018).
715 44. B. Li *et al.*, Drebrin restricts rotavirus entry by inhibiting dynamin-mediated
716 endocytosis. *Proceedings of the National Academy of Sciences of the United*
717 *States of America* **114**, E3642-E3651 (2017).
718 45. R. Guo *et al.*, Characterization and evaluation of the pathogenicity of a natural
719 recombinant transmissible gastroenteritis virus in China. *Virology* **545**, 24-32
720 (2020).
721 46. C. R. Bolen, S. Ding, M. D. Robek, S. H. Kleinstein, Dynamic expression profiling
722 of Type I and Type III Interferon-stimulated hepatocytes reveals a stable hierarchy
723 of gene expression. *Hepatology*, (2013).
724 47. S. Ding, W. Khoury-Hanold, A. Iwasaki, M. D. Robek, Epigenetic reprogramming
725 of the type III interferon response potentiates antiviral activity and suppresses
726 tumor growth. *PLoS biology* **12**, e1001758 (2014).
727
728

729 **Funding**

730

731 This study is supported by the National Institutes of Health (NIH) DDRCC grant P30
732 DK052574, NIH grants K99/R00 AI135031 and R01 AI150796 and the COVID-19 Fast
733 Grants Funding to S.D., NIH contracts and grants (75N93019C00062 and R01 AI127828)
734 and the Defense Advanced Research Project Agency (HR001117S0019) to M.S.D., NIH
735 grant U01 AI151810 to A.C.M.B., and unrestricted funds from Washington University
736 School of Medicine and NIH grant R37 AI059371 to S.P.W. The *in vivo* pig studies are
737 supported by the Jiangsu Province Natural Sciences Foundation (BK20190003) and
738 National Natural Science Foundation of China (31872481) to B.L. J.B.C. is supported by
739 a Helen Hay Whitney Foundation postdoctoral fellowship.

740

741 **Author contributions**

742

743 J.S., Q.Z., R.Z., and S.D. designed, executed, and analyzed *in vitro* efficacy studies.
744 M.F.G.C., H.P.K., and G.H. assisted with the RNA extraction and RT-qPCR analysis. Y.Z.
745 performed the *in vitro* TGEV inhibition studies. Z.L. performed the flow cytometry analysis.
746 L.C. wrote the algorithm that quantifies inhibitor screen results. P.W.R. and S.P.J.W.
747 constructed the VSV-SARS-CoV-2 virus. Q.Z., J.Z., and R.G. propagated and titrated
748 viruses. J.B.C. propagated and infected the clinical isolate of SARS-CoV-2. P.Y.S.
749 provided the recombinant SARS-CoV-2 mNeonGreen virus. A.L.B propagated the
750 mNeonGreen virus and designed the SARS-CoV-2 Taqman probe. S.H., B.L., and S.D.
751 designed the *in vivo* efficacy studies. S.H., J.Z., X.C., B.F., and B.N., performed the *in*

752 *vivo* TGEV infection experiments, dissected the animals and harvested tissues, and
753 measured viral titers and cytokine mRNA levels. X.W., S.P.J.W., M.S.D., A.C.M.B., B.L.,
754 and S.D. provided supervision and funding for the study. J.S. and S.D. wrote the
755 manuscript with the input and edits from S.H., Q.Z., J.B.C., J.Z., Z.L., M.F.G.C., H.P.K.,
756 G.H., S.P.J.W., M.S.D., A.C.M.B., and B.L.
757
758 **Competing interests**
759
760 The Boon laboratory has scientific research agreements with AI therapeutics, Greenlight
761 Biosciences and Nano Targeting & Therapy Biopharma Inc. M.S.D. is a consultant for
762 Inbios, Eli Lilly, Vir Biotechnology, NGM Biopharmaceuticals, and Emergent BioSolutions
763 and on the Scientific Advisory Boards of Moderna and Immunome. The Diamond
764 laboratory at Washington University School of Medicine has received unrelated
765 sponsored research agreements from Moderna, Vir Biotechnology, and Emergent
766 BioSolutions.
767
768 **Acknowledgements**
769
770 The authors thank Dr. Harry Greenberg (Stanford University, USA) and Dr. Bolívar A.
771 Villacís-Bermeo (Guayaquil, Guayas, Ecuador) for constructive comments and
772 arguments. We appreciate the assistance from Matthew Williams (Department of
773 Molecular Microbiology Media and Glassware Facility) and Erica Lantelme (Department

774 of Pathology and Immunology, Flow Cytometry Core Facility). Cytation plate scanning
775 was assisted by Zhou Huang (Department of Molecular Microbiology).
776
777 **Data and materials availability**
778
779 All raw data and statistical analysis in the current study are available in Table S3 and
780 Dataset S1. RNA-seq dataset has been deposited onto NCBI GEO (GSE156219).